Theory of action potentials

Romain Brette

March 14, 2017

Contents

Chapter 4

Excitability of an isopotential membrane

In this chapter, we address theoretical questions such as: under what conditions is a membrane excitable? what determines the threshold for spike initiation? We focus on the excitability of an isopotential membrane, such as the membrane of the space-clamped squid giant axon. The situation is different in neurons since action potentials are initiated in a small axonal region next to the cell body (the axonal initial segment), as we will see in chapter **??**, but the same concepts will be used and some results also apply.

4.1 Elements of dynamical systems

4.1.1 What is a dynamical system?

The relevant mathematical framework to understand excitation is dynamical systems theory. A *dynamical system* is defined by a space of possible states s, and a rule that describes how the state of the system evolves in time. We call this evolution a trajectory $s(t)$. Importantly, at any given moment t_0, the future trajectory $s(t), t \geq t_0$, is entirely determined by the present state $s(t_0)$[1].

[1] In a random dynamical system, the future trajectory is not fully determined by the present state; however, we consider that all the information we have about future trajectories is contained in the knowledge of the present state $s(t_0)$.

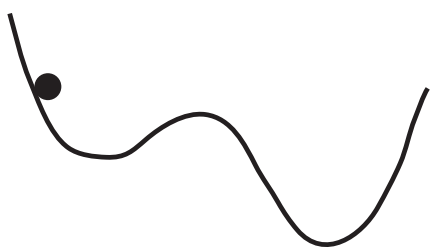

Figure 4.1: Example of a dynamical system.

An example is a ball rolling on a landscape (Figure 4.1). What is the state of this dynamical system? We note that the future trajectory of the ball is not entirely determined by its position: here the ball might be going down or going up. But according to Newton's laws, the future trajectory is completely determined if we know both the position and the (signed) velocity of the ball[2]. Thus the state is characterized by two real numbers, which makes it a two-dimensional dynamical system[3]. The Hodgkin-Huxley model is a 4-dimensional dynamical system, since it has 4 state variables: membrane potential V and gating variables m, h and n. It also has many parameters (e.g. capacitance), which do not count as state variables because they are constant (just as the mass of the ball).

The ball shown on Fig. 4.1 is an example of an excitable system. At a given moment it may be sitting on the higher valley. If the velocity is zero, then the ball will stay there forever. This state, defined by position = higher valley and velocity = 0, is called a *stable equilibrium*. We may then tap the ball, giving it some momentum. The tap is what we might call the stimulus in a biological experiment. This means changing the state of the ball (position = higher valley, velocity = positive number). If we tap gently, the ball will move up then go back to its initial state. If we tap more strongly, the ball might pass the hill and end up in the lower valley, which is also a stable equilibrium. There is a threshold in stimulus strength that distinguishes between two distinct behaviors of the system: converging to the higher valley, or converging to the lower valley. This is what we call an excitable system.

The most common mathematical formalism to describe dynamical systems in continuous time is differential equations[4]. If $\mathbf{x}$ is an n-dimensional vector representing the state of the system, then its evolution is constrained by:

$$\frac{d\mathbf{x}}{dt} = f(\mathbf{x})$$

Under some fairly broad conditions on the function f[5], this defines a dynamical system, that is, the future trajectory of $\mathbf{x}(t)$ only depends on the present state. All neural models discussed in this book are dynamical systems described by differential equations.

In this chapter, we will expose elementary concepts of dynamical system theory, as we will focus mostly on one-dimensional systems, simpler than a ball rolling on a landscape. There is however a large body of theoretical work on more advanced dynamical systems concepts applied to neural excitability, which we will briefly describe in section **??**.

4.1.2 Membranes as dynamical systems

Action potential models have at least two state variables

In an isopotential model, the membrane equation is a differential equation:

[2] or more precisely, position and momentum, which is mass times velocity.

[3] We assume that the ball always remains on the landscape. More generally, the ball is characterized by two vectors, and therefore the system is 4-dimensional (if the ball is constrained in a plane) or 6-dimensional.

[4] Discrete time would mean iterations of a map, as in an algorithm.

[5] given by the Cauchy–Lipschitz theorem.

$$\frac{dV}{dt} = f(V)$$

where $f(V)$ is the membrane current I_m divided by the membrane capacitance C. In general, f is actually also a function of other state variables, for example the gating variables m, n and h in the Hodgkin-Huxley model. Thus, it does not define a one-dimensional dynamical system. We obtain a one-dimensional system in the simple case of a passive membrane, that is, where permeabilities are fixed. For example, with a linear leak current (as in the Hodgkin-Huxley formalism):

$$\frac{dV}{dt} = \frac{g_L}{C}(E_L - V)$$

where C is membrane capacitance and g_L is leak conductance. Here, dV/dt is a function of V only: if we know $V(0)$, then we can deduce the full trajectory $V(t)$ at any future time. One simple consequence is that all trajectories are monotonous, either increasing or decreasing[6] (or constant). This is a general property of all one-dimensional dynamical systems[7]. In particular, action potentials cannot be modeled by a one-dimensional dynamical system, because an action potential is not monotonous: V increases then decreases. Thus we need at least two state variables to make an action potential model[8].

Spike initiation can be modeled as a one-dimensional dynamical system

Although a full action potential cannot be modeled by a one-dimensional system, the *initiation* of action potentials can, with a few approximations[9]. First, we neglect voltage-gated K+ channels. That is, we assume that they do not open on the time scale of interest (the initial rising phase of the action potential). Empirically, this indeed appears to be approximately the case for the squid axon (figure 4.2) and cortical pyramidal cells (figure 4.3). In this chapter, we will simply assume that they are closed. However, to obtain a one-dimensional description, it is sufficient to assume that K^+ permeability is fixed (but not necessarily zero). Theoretically, there is a functional reason why the K^+ current should start only near the peak of the action potential: this situation is energetically favorable since the K^+ current opposes the Na^+ current (with a positive K^+ current, more Na^+ flux would be needed for the same net current). We will examine the energetic question in more detail in chapter **??**; let us simply mention for now that there can be a significant overlap between the Na^+ and K^+ currents, but mostly in the falling phase of the action potential (see Figs 4.2 and 4.3, and Carter and Bean (2009)). This first approximation implies that we can model spike initiation with a simplified membrane equation:

$$\frac{dV}{dt} = \frac{1}{C}\Big(I_L + I_{Na}\Big)$$

[6]Indeed, if a trajectory were increasing then decreasing, then there would be a value of V at which we have both $f(V) > 0$ and $f(V) < 0$.

[7]defined by differential equations.

[8]Two classical two-dimensional models of action potentials are the Fitzhugh-Nagumo model (Nagumo et al., 1962) and the Morris-Lecar model (Morris and Lecar, 1981).

[9]These approximations are not reasonable for all excitable cells, as we will see when we discuss excitability types in section **??**.

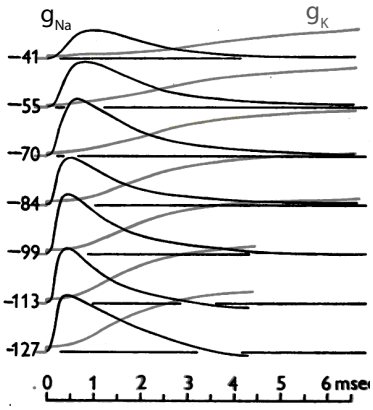

Figure 4.2: Overlap of Na^+ and K^+ conductances in squid axon (adapted from Hodgkin and Huxley (1952b)). The axon is clamped at the voltages indicated on the left, relative to the resting potential (with the convention $V = -V_m$).

where I_L and I_{Na} are leak and Na^+ currents, respectively.

The second approximation consists in assuming that the Na^+ current is an instantaneous function of V, $I_{Na}(V)$. We then obtain a one-dimensional dynamical system:

$$\frac{dV}{dt} = f(V) \equiv \frac{1}{C}\Big(I_L(V) + I_{Na}(V)\Big)$$

There are different ways to justify this approximation. One is phenomenological: we simply look for the best fitting one-dimensional model. For example, in figure 4.4, a cortical neuron is stimulated with a white noise current $I(t)$, strong enough to make the neuron spike. We then look for $f(V)$ such that

$$\frac{dV}{dt} \approx f(V) + \frac{I(t)}{C}$$

in a least-square sense[10] (Badel et al., 2008; Harrison et al., 2015). We can see on the figure that $f(V)$ is approximately linear below -45 mV, which presumably corresponds to the leak current $I_L(V)$ (divided by C), and above -40 mV there is a strong membrane current that presumably corresponds to the Na^+ current $I_{Na}(V)$. As we will see in more detail in section 4.3.3, this current is approximately exponential near spike initiation (see inset in figure 4.4).

Another way to justify the one-dimensional approximation is to consider the time scales of the different processes. If we assume that 1) inactivation develops only well after the initiation of the action potential (similarly to the K^+ current), and 2) the time constant of Na^+ channel activation is short, compared to the time scale of spike initiation, then we can consider that I_{Na} is effectively an instantaneous function of V. In the Hodgkin-Huxley model, this amounts to replacing the gating variable m by its steady-state value $m_\infty(V)$, and the inactivation variable h by its initial value h_0. Figure 4.5A shows that, at 23 °C,

[10] That is, $f(V)$ is the average of $dV/dt - I(t)/C$, for all the instants when the membrane potential is V.

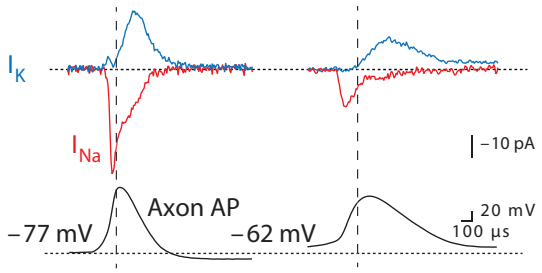

Figure 4.3: Overlap of Na^+ and K^+ currents in an axonal patch of membrane during an action potential, in a layer 5 pyramidal cortical neuron (adapted from Hallermann et al. (2012)). The axonal patch (outside-out configuration) is voltage-clamped at a time-varying value corresponding to a previously measured action potential, with the neuron depolarized to either -77 mV or -62 mV. Currents are isolated with ion channel blockers. In both cases, there is little K^+ current during the initial phase of the spike.

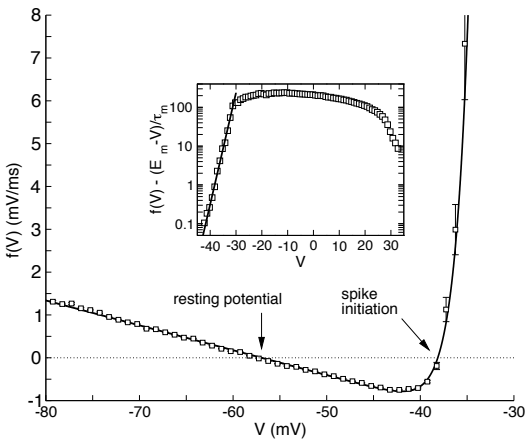

Figure 4.4: Average membrane current (divided by capacitance) as a function of membrane potential during white noise stimulation of a cortical neuron (adapted from Badel et al. (2008)). The inset shows $f(V)$ in logarithmic scale, over a more depolarized range (-45 to 35 mV).

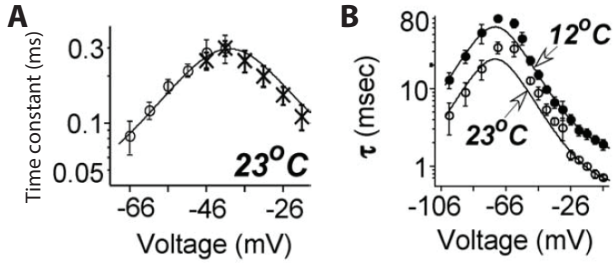

Figure 4.5: Time constant of activation (A) and inactivation (B) in prefrontal cortical neurons (adapted from Baranauskas and Martina (2006)).

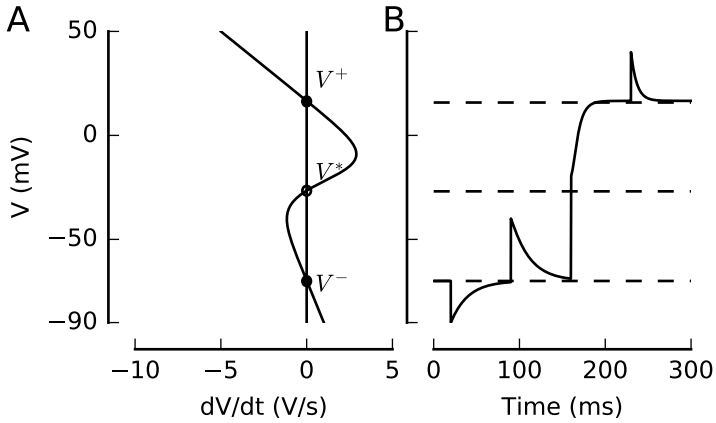

Figure 4.6: A one-dimensional model of an excitable membrane. A, The model is defined by $dV/dt = f(V)$. Stable equilibria are marked with filled disks, the unstable equilibrium with an open disk. B, Simulated current-clamp experiment, where the membrane potential is moved instantaneously to 4 different values.

the maximum activation time constant is about 0.3 ms in prefrontal cortical neurons (Baranauskas and Martina, 2006). At physiological temperature, one would expect this maximum value to be smaller than 0.1 ms. Inactivation is roughly two orders of magnitude slower (Fig. 4.5B). In the spike initiation region (around −50 mV), inactivation is still quite slow compared to the action potential rise (5-10 ms at 23 °C) and therefore we do not expect it to be a major determinant of the initial Na^+ current.

We will look at specific one-dimensional models in section 4.3, but for the moment we can consider for example that $C.f(V)$ corresponds to the "early current" shown in Fig. **??**B and **??**B, or to the average current shown in Fig. 4.4.

4.1.3 Equilibria

Let us consider a one-dimensional dynamical system defined by $dV/dt = f(V)$, which could be the membrane equation of an excitable cell, with $f(V) = I/C$. Figure 4.6A shows an example, which is similar to the early current shown in Fig. **??**B for the squid axon and in Fig. **??**B for Paramecium, but modified to be more readable. The graph of f can be used to predict the evolution of $V(t)$: if $dV/dt = f(V) > 0$, then $V(t)$ will increase; if $f(V) < 0$, then $V(t)$ will decrease. We will call this graph the *excitability curve*. This is illustrated in the simulated current-clamp experiment shown in Fig. 4.6B, where we instantaneously depolarize or hyperpolarize the membrane at different times. Physically, it corresponds to delivering electrical shocks at different times.

An *equilibrium* or fixed point is a value of the state variable V such that $f(V) = 0$, so that $V(t)$ remains constant. There are three equilibria in the model of Fig. 4.6. The lowest one, V^-, corresponds to the resting potential. If the system is moved in the neighborhood of V^-, as shown on Fig. 4.6B, then $V(t)$ converges back to V^-. This is called a *stable equilibrium*. In this model, V^+ is also a stable equilibrium, and corresponds to the peak of the action potential. On the contrary, V^* is an *unstable equilibrium*: when the system is perturbed around V^*, $V(t)$ moves away from V^*, towards one of the two stable equilibria V^- and V^+. More precisely, an equilibrium is called unstable when it is not stable, i.e., there is at least one direction of perturbation where the system moves away from the equilibrium.

What is the condition for an equilibrium to be stable? This is clear from the excitability curve (graph of f) shown in Fig. 4.6A. We have $f(V) = dV/dt > 0$ just below V^- and $f(V) = dV/dt < 0$ just above V^-, so in both cases $V(t)$ evolves towards V^-. This situation is obtained when $f'(V) < 0$[11]. Conversely, an equilibrium is unstable when $f'(V) > 0$. In the model shown in Fig. 4.6, the unstable equilibrium V^* splits the state space[12] (all possible values for V) into the two *basins of attraction* of the stable equilibria V^- and V^+. The basin of attraction of a stable equilibrium is the set of initial conditions $V(0)$ such that trajectories $V(t)$ converge to that equilibrium. Thus, an unstable equilibrium defines the notion of a *threshold*: below V^*, trajectories converge towards the resting potential V^-; above V^*, trajectories converge towards the action potential peak V^+. This definition corresponds to a current-clamp experiment in which an electrical shock is instantaneously applied to the membrane, and then the membrane potential evolves with no stimulus. We will look at other possible definitions of threshold in section 4.2.

[11] Proof: a Taylor expansion in the neighborhood of V^- gives $f(V) \approx f(V^-) + f'(V^-)(V - V^-) = f'(V^-)(V - V^-)$. Thus if $f'(V^-) < 0$ then dV/dt has the sign of $V^- - V$. This is a necessary but not sufficient condition, because of the special case $f'(V^-) = 0$, for example with $f(V) = -V^3$. Using a Taylor expansion, one can see that more generally, a stable equilibrium is when there is an odd integer p such that $f^{(k)} = 0$ for all $k < p$ and $f^{(p)} < 0$. However, we will not encounter this situation in this chapter.

[12] In one-dimensional systems, there is always an unstable equilibrium between two stable equilibria, as is graphically intuitive from Fig. 4.6A. Proof: if V^- is a stable equilibrium, then $f(V) < 0$ just above V^-; if $V^+ > V^-$ is a stable equilibrium, then $f(V) > 0$ just below V^+. Therefore there is a point V^* in between such that $f(V^*) = 0$. If we pick the lowest such point, then we must have $f(V) < 0$ just below V^*, therefore V^* cannot be stable.

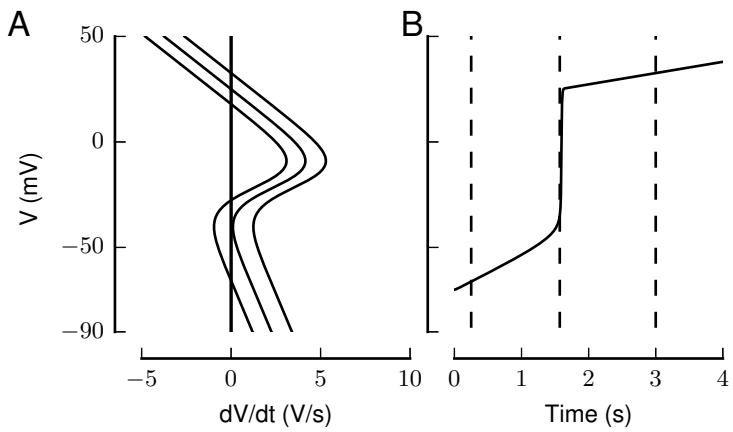

Figure 4.7: Bifurcation in a one-dimensional model of an excitable membrane. A, The model is defined by $dV/dt = f(V) + I_e/C$, where I_e is an injected current. The graph is for 3 different values of I_e (increasing from left to right). B, Simulated current-clamp experiment, where current I_e is slowly increased. The dashed lines correspond to the 3 curves shown in A. A spike is initiated at the bifurcation point, when the graph shown in A is tangent to the line $dV/dt = 0$.

4.1.4 Bifurcations

Another powerful concept in dynamical system theory is *bifurcation*. A bifurcation is a change in the number or nature of equilibria. Suppose that we inject a steady current I_e in the cell (the e subscript is for electrode or external), as shown in Fig. 4.7. The membrane equation is then:

$$\frac{dV}{dt} = f(V) + \frac{I_e}{C} \equiv g(V, I_e)$$

Now dV/dt depends on the state variable V and on the parameter I_e. We start with a current $I_e = 0$: the membrane potential sits at the resting potential V^-. As we slowly increase I_e, the equilibrium value V^- increases and $V(t)$ follows it, since it is a stable equilibrium. At some point, V^- becomes unstable and disappears (middle curve in Fig. 4.7A). What happens then is that the membrane potential $V(t)$ increases towards the next stable equilibrium V^+ (middle dashed line in Fig. 4.7B). This particular type of bifurcation is called a *saddle-node bifurcation*: two equilibria collide and annihilate each other (the resting potential and the unstable equilibrium).

We can see that the bifurcation occurs when the excitability curve (graph of dV/dt vs. V) is tangent to the line $dV/dt = 0$ (Fig. 4.7A). Mathematically, this means:

$$\begin{aligned} g(V, I_e) &= 0 \\ \frac{\partial g}{\partial V}(V, I_e) &= 0 \end{aligned}$$

There are two equations and two unknowns, and so this couple of equations allows us in principle to deduce the values of V and I_e where the bifurcation

occurs, called the *bifurcation point*[13]. The beauty of bifurcation theory is it applies to the change of any parameter. For example, imagine we slowly increase the density of Na^+ channels, starting from an inexcitable cell. At the beginning there is a single stable equilibrium, but then at some point a new stable equilibrium appears, together with an unstable equilibrium. This point where the cell becomes excitable is a bifurcation point (again a saddle-node bifurcation). If we keep on increasing channel density, at some point the resting potential will disappear and there will be a single stable equilibrium: the system goes through a second saddle-node bifurcation. Bifurcation is a very general and useful concept: every time we are considering a situation where a graded change in a parameter results in a discrete change in behavior, we are looking at a bifurcation. Bifurcation theory gives us simple mathematical tools to calculate when these changes occur. In the following, we will apply it to stimulus strength, to Na^+ conductance and to properties of the Na^+ channels.

4.2 The threshold

4.2.1 Different ways to excite a membrane

In the previous section, we have seen two ways to excite a membrane. The first way was to deliver an instantaneous electrical shock of charge Q, as in Fig. **??**. The effect is to instantaneously shift the potential by Q/C, as shown on Fig. 4.6B[14]. If the membrane is initially at rest ($V = V^-$), then this stimulus brings the potential to $V^- + Q/C$. Then $V(t)$ will evolve towards one of the two stable equilibria, depending on whether $V^- + Q/C > V^*$. Thus we can define a threshold for voltage, which is the unstable equilibrium V^*, and a threshold for stimulus strength, in this case a charge threshold, equal to:

$$Q^* = C(V^* - V^-)$$

This is the minimum charge necessary to trigger an action potential. Another way to excite a membrane is to deliver a steady current I_e and increase it slowly, as in section 4.1.4. Again we can define a threshold for stimulus strength, this time a current threshold I_e^*, which can be calculated using the bifurcation equations (see section 4.1.4). This current threshold is called *rheobase*. We can also define a voltage threshold, as the membrane potential at the bifurcation point. This is the maximum membrane potential that can be reached without eliciting a spike. While this definition also applies to the voltage threshold we have defined for instantaneous shocks, the value of the voltage threshold is different in the two cases. For instantaneous shocks, the voltage threshold is a solution to $f(V) = 0$; for steady currents, the voltage threshold is a solution to $f'(V) = 0$. These two equations have different solutions.

This can be seen in Fig. 4.7A. A voltage threshold for instantaneous shocks can be defined for a low value of I_e, corresponding to the first curve on the left. As we have seen, this threshold is the unstable equilibrium, the second point

[13] Note that there are actually two such solutions.

[14] using the physical relation $Q = CV$ that defines capacitance. Alternatively, one can define the injected current as $I_e(t) = Q\delta(t)$, where $\delta(t)$ is the Dirac function such that $\delta(t) = 0$ when $t \neq 0$ and $\int \delta = 1$. One can check that indeed $\int I_e = Q$. Then integrating the membrane equation over a small time gives $\Delta V = Q/C$.

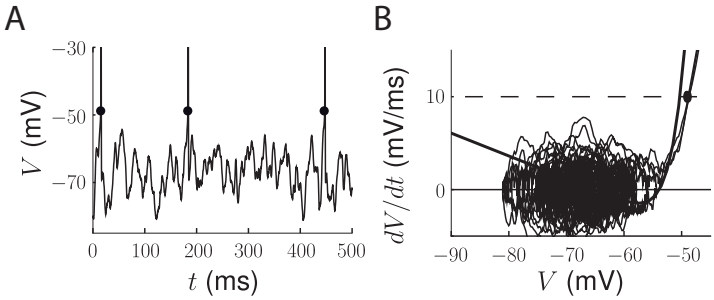

Figure 4.8: Spike onset (adapted from Platkiewicz and Brette (2010)). A, Simulated trace of a Hodgkin-Huxley-type model with noisy injected current (representing synaptic inputs), with spike onset measured by the first derivative method. B, Representation of the trace in (A) in phase space, showing dV/dt vs. V. The first derivative method consists in measuring the membrane potential V when the derivative crosses a predefined value (dashed line) shortly before an action potential. The trace is superimposed on the excitability curve $dV/dt = (f(V) + I_0)/C$, which defines the dynamics of the model. I_0 is the mean input current, so that trajectories in phase space fluctuate around this excitability curve.

where the excitability curve crosses the line $dV/dt = 0$. On the other hand, the voltage threshold for a slowly increasing current I_e corresponds to the point where the excitability curve is tangent to the line $dV/dt = 0$ (second curve). It appears that this voltage threshold is lower. In other words, in a one-dimensional model of excitable membrane, the voltage threshold for electrical shocks is higher than the voltage threshold for steady currents[15]. In the following, we will refer to the voltage threshold for instantaneous shocks as the threshold for fast inputs, the voltage threshold for steady currents as the threshold for slow inputs.

Thus, in general the voltage threshold is a concept that depends on the type of stimulation; there is no voltage threshold independent of stimulation (Koch et al., 1995). We will see however that this can be different when we take into account the geometry of the spike initiation system, in particular the fact that spikes are initiated in a small axonal region next to the cell body (chapter **??**).

4.2.2 Spike onset

In the experimental literature, the terms *spike threshold* are often used to refer to a measurement of the voltage at the onset of action potentials. Figure 4.8A shows the simulated membrane potential of model of the Hodgkin-Huxley type (same type of equations, but different models for the ionic currents), where a noisy current representing synaptic inputs is injected. The spike onset is measured using the *first derivative method*, which consists in measuring the membrane potential V when its derivative dV/dt crosses an empirical criterion (Azouz and Gray, 1999; Kole and Stuart, 2008) (Fig. 4.8B). Other methods have been used to measure spike onset (Sekerli et al., 2004). The second and

[15] We will see in chapter **??** that this can be different when Na^+ channel inactivation is taken into account.

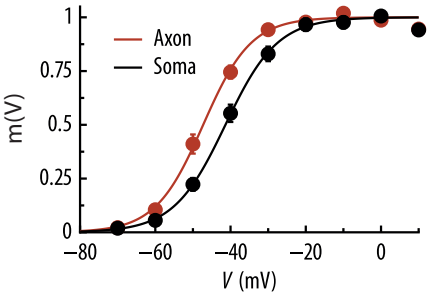

Figure 4.9: Activation curve of Na^+ channels of hippocampal granule cells, in axon and soma (adapted from Schmidt-Hieber and Bischofberger (2010)). It is obtained from the peak current measured in an activation voltage-clamp protocol.

third derivative methods consist in measuring V when respectively d^2V/dt^2 and d^3V/dt^3 reach their maximum (Henze and Buzsaki, 2001; Wilent and Contreras, 2005). Sekerli et al. (2004) compared those methods by asking electrophysiologists to identify spike onsets by eye on several membrane potential traces. They found that visual inspection was best matched by the first derivative method, although that method critically relies on the choice of the derivative criterion.

If Na^+ channels opened as a step function of membrane potential, then spike onset and the various definitions of voltage threshold (fast and slow inputs) would all be identical. However, this is not the case in general. In Fig. 4.8B, we see that the spike onset defined by the first derivative method is higher than both the threshold for fast inputs (intersection of excitability curve and line $dV/dt = 0$) and for slow inputs (minimum of the excitability curve). Nonetheless, spike onset is often used as a proxy for spike threshold (in particular of its dynamics, see chapter **??**) because these can be quantitatively related to each other when the excitability function $f(V)$ is known (Platkiewicz and Brette, 2010). Further arguments will be given in chapter **??**, where we will see that axonal Na^+ channels open as a step function of somatic membrane potential.

4.3 Three simplified models of excitability

We have seen in section 4.1.2 that spike initiation can be (approximately) modeled by a one-dimensional dynamical system. Here we will examine three simplified models that will allow us to make analytical calculations.

4.3.1 The sharp model

The simplest model consists in assuming that Na^+ channels open as a step function of membrane potential. If we define $m(V)$ as the proportion of open channels as a function of V, then:

$$m(V) = H(V - V_{1/2})$$

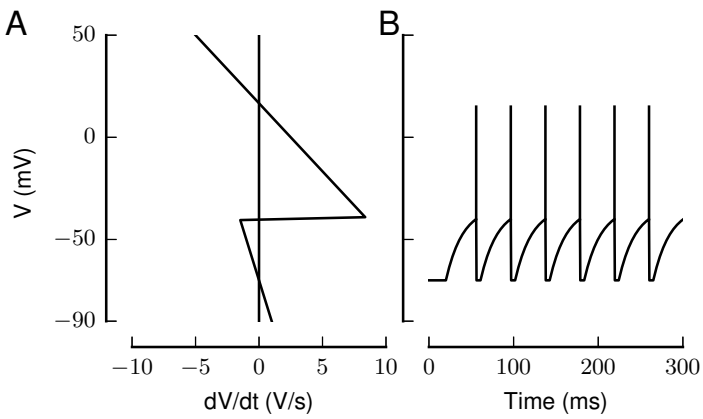

Figure 4.10: The sharp model of excitability. A, Excitability curve of the sharp model, with $V_{1/2} = -40$ mV. B, Simulated membrane potential trace of an integrate-and-fire model, responding to a step current.

where H is the Heavyside function[16] and $V_{1/2}$ is called the *activation voltage* or *half-activation voltage* (the reason for these terms will be clearer in the next section). Figure 4.9 shows $m(V)$ vs. V, which we will call the *activation curve* of the Na^+ channels, for granule cells of the hippocampus (from Schmidt-Hieber and Bischofberger (2010)). To obtain this curve, the peak Na^+ current is measured with an activation protocol in voltage-clamp, and is then divided by the driving force $(E_{Na} - V)$ to obtain a conductance $g(V)$[17]. The conductance is then divided by the maximum conductance to obtain $m(V) \equiv g(V)/\max g$. The measured function $m(V)$ is clearly not a step function, but if we consider the entire relevant voltage range, from -80 mV to the reversal potential of Na^+ ($E_{Na} \approx 50$ mV), we may (roughly) approximate $m(V)$ by a step function with activation voltage $V_a \approx -40$ mV (for the somatic channels) or -50 mV (for the axonal channels).

This is of course a very crude approximation, but it will help us develop some intuition. To be more specific, we will consider a model with linear currents as in the Hodgkin-Huxley model, so that the membrane equation is:

$$C\frac{dV}{dt} = g_L(E_L - V) + g_{Na}H(V - V_{1/2})(E_{Na} - V)$$

where the first term is the leak current I_L and the second term is the Na^+ current. The excitability curve is represented on Figure 4.10A. Most of our analysis is directly applicable to other permeability models, in particular GHK theory.

In the sharp model, the various definitions of voltage threshold and spike onset match and correspond to the activation voltage $V_{1/2}$. This corresponds to a simple neuron model known as the *integrate-and-fire model*. The integrate-and-fire model is a phenomenological neuron model, first introduced by Lapicque

[16] such that $H(x) = 1$ if $x > 0$ and $H(x) = 0$ otherwise.

[17] Note that it is implicitly assumed that the Na^+ current follows a linear current-voltage relation as in the Hodgkin-Huxley model, but this may not be correct.

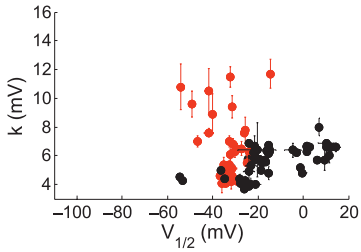

Figure 4.11: Activation properties of Na^+ channels, showing Boltzmann slope factor k vs. half-activation voltage $V_{1/2}$ in a number of rat Na^+ channels, collected from various channel subtypes and experimental preparations (adapted from Angelino and Brenner (2007)). Black: neuronal channels; red: muscular channels.

(1907), which is defined by a membrane equation without voltage-dependent ionic channels:

$$C\frac{dV}{dt} = g_L(E_L - V) + I_e$$

where I_e is an injected current. A spike is triggered when V reaches some threshold value V_t (corresponding to $V_{1/2}$ in the sharp model), then the membrane potential is instantaneously reset to a value V_r and maintained there for a refractory period Δ (Fig. 4.10B).

Since in this chapter we are only interested in spike initiation, we will discuss only the spike initiation component of the integrate-and-fire model, which we call the sharp model of spike initiation.

4.3.2 The Boltzmann model

A more accurate model is the *Boltzmann model*, where the Na^+ channel activation curve $m(V)$ is modelled as a *Boltzmann function*. On Figure 4.9, the curves are fits of Boltzmann functions to patch-clamp measurements of the activation curve (peak conductance vs. V, relative to maximum conductance). Measurements are indeed generally well fitted by a Boltzmann function, which is defined as:

$$m(V) \equiv \frac{1}{1 + e^{(V_{1/2} - V)/k}}$$

where $V_{1/2}$ is the *half-activation voltage*, such that $m(V_{1/2}) = 1/2$, and k is the *Boltzmann slope factor*. Figure 4.6A shows the excitability curve of a Boltzmann model (including a leak current). The slope factor k quantifies the voltage range over which the channels open. Specifically, the proportion of open channels goes from about 1/4 at voltage $V_{1/2} - k$ to about 3/4 at voltage $V_{1/2} + k$. The sharp model is obtained is the limit $k \to 0$ mV. Figure 4.11 gives typical values for $V_{1/2}$ and k.

It is important to realize that these channel properties can vary between cells and even within a cell, because there is no such thing as "the Na^+ channel". First, there are 9 subtypes of voltage-gated Na^+ channels (named Nav1.1 to Nav1.9), each corresponding to one gene coding the main protein, called α-unit. A channel is made of an α-unit and additional proteins called β-units.

Channel properties depend on the expression of β-units. In addition, the α-unit can be altered by alternative splicing (different versions of the gene) and by phosphorylation (Levitan, 1994), that is, post-translational alterations of the protein. Therefore, values shown in Fig. 4.11 and individual studies should be understood as general orders of magnitude.

An additional value of the Boltzmann model is it can be derived from a simple biophysical model. If we assume that the channel can be in two states (open and closed) with different potential energies, then according to mechanical statistics the probability that the channel is in the open state is:

$$m(V) = \frac{1}{1 + e^{\frac{\Delta E}{k_B T}}}$$

where ΔE is the potential energy difference between the two states, k_B is the Boltzmann constant (about 1.38×10^{-23} J.K^{-1}) and T is absolute temperature in Kelvin. The potential energy difference includes the difference in electrical potential energy and a voltage-independent term ΔE_0 which reflects the difference in protein conformation. A difference in electrical potential energy can arise if charges are moved when the protein changes state, and it will then be proportional to the membrane potential[18]. For example, if in the closed state the channel has a charge q on the external side of the membrane, which is then moved to the internal side of the membrane in the open state, then the potential energy difference is qV. The proportion of open channels would then be:

$$m(V) = \frac{1}{1 + e^{\frac{qV + \Delta E_0}{k_B T}}}$$

Thus we obtain the Boltzmann model of Na^+ channel activation, where the Boltzmann slope factor k is related to the number of charges that are moved when the channel opens. Hodgkin and Huxley used this reasoning to propose that the channel carries 6 negative elementary charges (Hodgkin and Huxley, 1952a).

Although the Boltzmann model is theoretically appealing and has some empirical support, it should not be forgotten that it totally neglects the dynamics of channel opening, as for the other simplified models we consider in this chapter. There is another, more subtle, qualification to be made to the fact that patch-clamp measurements of Na^+ channel activation curves are well fitted by Boltzmann functions. Fits to experimental data are done on large voltage ranges, which go well beyond the spike initiation region (-80 to 10 mV in Figure 4.9). This means that the fit is mostly sensitive to the shape of the empirical curve where it varies most, i.e., near half-activation voltage. The match may not be excellent in the region that is most relevant for spike initiation, and where the data are noisier (because currents are smaller). This problem is illustrated on Figure 4.12, which shows on the activation curve of an empirical model of Na^+ channels how the fitting results depend on the voltage region chosen for the fit (a three-fold variation in estimated k). This issue arises in part from the fact that many Na^+ channel models use several activation gates, as in the Hodgkin-Huxley model, which uses 3 (the m^3 factor). If the equilibrium function of each gate ($m_\infty(V)$) is a Boltzmann function, then the activation curve is not exactly

[18] at least in a constant field model.

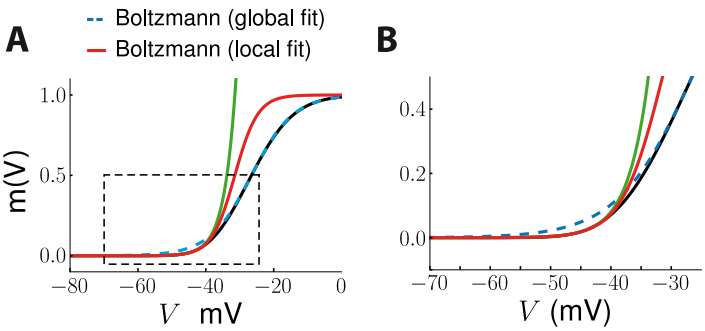

Figure 4.12: Fitting the Na activation curve to a Boltzmann function (adapted from Platkiewicz and Brette (2010)). A, The Na channel activation curve of a Hodgkin-Huxley type model (black line) was fit to a Boltzmann function on the entire voltage range (dashed blue line) and on the spike initiation range only (−60 mV to −40 mV, red line). The green line shows the exponential fit on the spike initiation range. B, In the hyperpolarized region (zoom of the dashed rectangle in A), the global Boltzmann fit (dashed blue line) is not accurate, while the local Boltzmann fit and the local exponential fit better match the original curve.

a Boltzmann function ($m_\infty^3(V)$). In addition, the activation curve is measured from the peak current in a voltage-clamp experiment, which means that the measurements may be influenced by the development of inactivation (see for example Fig. 10 in Platkiewicz and Brette (2010)).

In this chapter, we will use the Boltzmann model with a linear current-voltage relation, that is:

$$C\frac{dV}{dt} = g_L(E_L - V) + g_{Na}m(V)(E_{Na} - V)$$

where $m(V)$ is a Boltzmann function. It is of course possible to consider the Boltzmann model of Na^+ channel activation with the GHK model of currents.

4.3.3 The exponential model

The third simplified model we will consider is the *exponential model*. It was introduced by Fourcaud-Trocme et al. (2003) as an approximation of models of the Hodgkin-Huxley type that allows analytical calculations. It is based on the Boltzmann model. In the hyperpolarized range, that is, when $V << V_{1/2}$, the Boltzmann function can be approximated by an exponential function:

$$m(V) \approx e^{(V-V_{1/2})/k}$$

as shown on Fig. 4.12 (green curve). However, as noted in section 4.3.2, Boltzmann functions are fitted to empirical measurements over a large voltage range, not on the hyperpolarized range. Nevertheless, Figure 4.13 shows that in the squid axon, the peak Na^+ conductance is indeed relatively well fitted by an exponential function of voltage in the low voltage range, here between the resting potential and about 20 mV above it (Hodgkin and Huxley, 1952b). In cortical

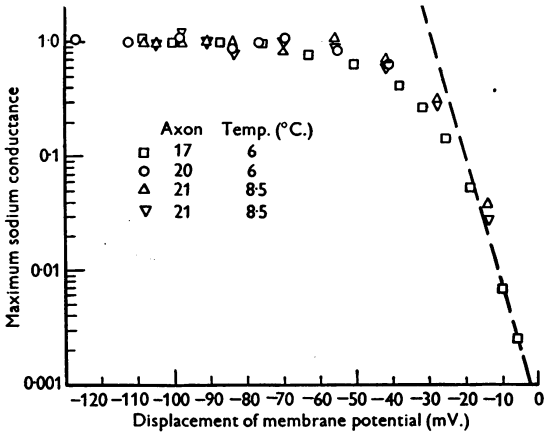

Figure 4.13: Na^+ activation curve of the squid axon shown in logarithmic scale, fitted by an exponential function (dashed line) (Hodgkin and Huxley, 1952b), with a slope factor $k \approx 4$ mV. The horizontal axis shows $V_0 - V_m$, where V_0 is the resting potential.

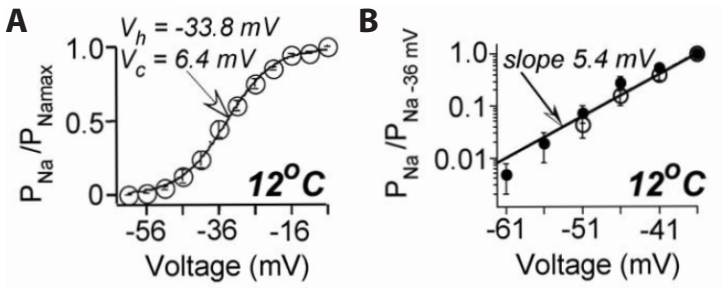

Figure 4.14: Na^+ activation curve of a pyramidal neuron of the prefrontal cortex (A), with the hyperpolarized region shown in logarithmic scale (B) (adapted from Baranauskas and Martina (2006)). Relative permeability is obtained based on the GHK model.

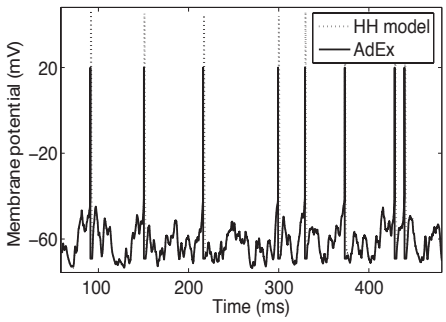

Figure 4.15: Simulated voltage trace of an adaptive exponential model (AdEx) fitted to a Hodgkin-Huxley type model, in response to a noisy current (adapted from Brette and Gerstner (2005)).

neurons, Na^+ permeability is well fitted by a Boltzmann function of voltage on a large range (Fig. 4.14A), and by an exponential function of voltage with similar slope factor in the hyperporalized range (Fig. 4.14B) (Baranauskas and Martina, 2006)).

With the linear model of currents, the Na^+ current is then:

$$I_{Na} = g_{Na} e^{(V-V_{1/2})/k}(E_{Na} - V)$$

We make a further approximation, by replacing V by $V_{1/2}$ in the driving force. By making this approximation, we introduce a relatively small error. Indeed, far below spike threshold, this current is very small, and therefore the error has little effect. Near threshold, we make a relative error of $(V_{1/2} - V)/(E_{Na} - V_{1/2})$; with $E_{Na} = 60$ mV, $V = -50$ mV and $V_{1/2} = -30$ mV, we obtain about 20%. Thus the membrane equation of the exponential model is:

$$C\frac{dV}{dt} = g_L(E_L - V) + g_{Na} e^{(V-V_{1/2})/k}(E_{Na} - V_{1/2})$$

Again this can easily be extended to the GHK model of currents. An interesting aspect of this model is it is also the basis of an integrate-and-fire type model. In this model, when a spike is initiated, the membrane potential diverges to infinity in finite time. An integrate-and-fire model can then be defined by considering that spike timing is the time of divergence, and the membrane potential is reset to some value after this event. This is called the *exponential integrate-and-fire model* (Fourcaud-Trocme et al., 2003). This model can be fitted to models of the Hodgkin-Huxley type and can reproduce their response relatively accurately[19], as shown on Fig. 4.15 (Brette and Gerstner, 2005). Variations of this model are also able to predict spike trains of real cortical neurons on a millisecond basis, when stimulated by noisy currents injected at the soma (Badel et al., 2008; Rossant et al., 2010, 2011; Harrison et al., 2015).

The exponential model has the same limitations as the Boltzmann model (e.g. it is a one-dimensional model), and in addition it is only relevant to examine spike initiation, since the Boltzmann function is approximately exponential in the hyperpolarized range only.

[19]with an additional equation that models voltage- and spike-triggered adaptation.

4.4 What determines the threshold?

4.4.1 The threshold equation

What is the relation between the various biophysical parameters (Na^+ and leak conductances, Na^+ channel properties) and the value of the spike threshold? In the sharp model, the voltage threshold is the half-activation voltage $V_{1/2}$, independently of the way the neuron is stimulated (Fig. 4.10). In other models, as we have seen in section 4.2, a voltage threshold can be defined as the maximum membrane potential that can be reached without triggering a spike, but its value depends on the type of stimulation.

For simplicity, we will consider the exponential model. An analysis of the Boltzmann model can be found in appendix **??**; the results are very similar. The membrane equation with a stimulating current I is:

$$C\frac{dV}{dt} = g_L(E_L - V) + g_{Na}e^{(V-V_{1/2})/k}(E_{Na} - V_{1/2}) + I$$

First, we multiply by the membrane resistance $R = 1/g_L$, and we rewrite the Na^+ driving force in units of k so as to make a unitless factor appear in front of the exponential:

$$\tau\frac{dV}{dt} = E_L - V + k\frac{g_{Na}}{g_L}\Big(\frac{E_{Na} - V_{1/2}}{k}\Big)e^{(V-V_{1/2})/k} + RI$$

We then insert this unitless factor in the exponential:

$$\tau\frac{dV}{dt} = E_L - V + ke^{(V-\theta)/k} + RI$$

where

$$\theta = V_{1/2} - k\log\Big(\frac{g_{Na}}{g_L}\frac{E_{Na} - V_{1/2}}{k}\Big)$$

By this algebraic manipulation, we can see that the Na^+ current-voltage relation is voltage-shifted by a quantity θ, which captures the dependence to all parameters g_L, g_{Na}, $V_{1/2}$ and E_{Na}. In fact, θ is the threshold for slow inputs. This can be seen by solving $f'(V) = 0$, where $f(V)$ is the right handside of the differential equation. Thus we will call the formula for θ the *threshold equation*. It has been derived in Platkiewicz and Brette (2010).

As we have seen, the threshold depends on the type of stimulation. For example, the threshold for fast inputs is the solution of $f(V) = 0$, which gives a different value (see Platkiewicz and Brette (2010)). However, our algebraic manipulation shows that this value will still be a function of θ and k, and so θ does capture the relative contribution of the different biophysical parameters to excitability.

It is possible to calculate the threshold for slow inputs in the Boltzmann model, by solving $f'(V) = 0$. This calculation gives a slightly modified formula (see appendix **??**):

$$\theta_{\text{Boltzmann}} \approx V_{1/2} - k\log\left(\frac{g_{Na}}{g_L}\frac{E_{Na} - V_{1/2}}{k} - 1\right)$$

As we have already noted, the threshold for the sharp model is $\theta = V_{1/2}$. We can see that this is consistent with the threshold equation when k tends to 0 mV, for both the exponential model and the Boltzmann model.

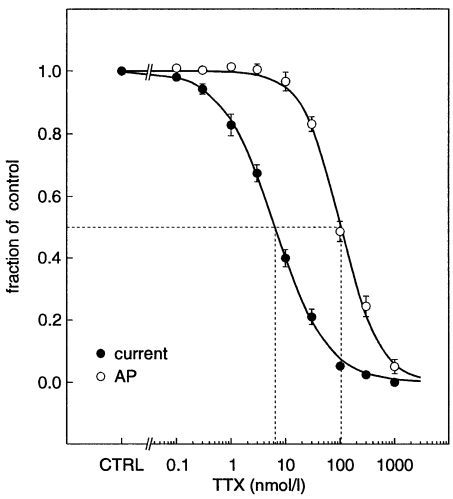

Figure 4.16: Dose-response curve of TTX, showing the fraction of available Na^+ channels as a function of TTX concentration in CA1 hippocampal neurons (black dots; from Madeja (2000)).

4.4.2 Experimental observations

Our theoretical analysis applies to isopotential models. However, as we will see in section **??**, the dependence of threshold on Na^+ channel properties should still be well captured by our analysis in the case when action potentials are initiated in the axonal initial segment. We expect this level of generality because the analysis relies on rewriting the Na^+ current so as to make a voltage shift appear in the current-voltage relation of the channels. However, our analysis does not include the specific role of geometrical factors, which we will examine later (section **??**). We now examine a few experimental observations that are relevant to the threshold equation. As we will see, current experimental data do not allow us to test very precise predictions, only general orders of magnitude.

Blocking Na^+ channels

The equation predicts that the spike threshold varies with g_{Na} as $-k \log g_{Na}$. As we have pointed out in section 4.3.2, there is some uncertainty about the value of k, but the order of magnitude should be about 5 mV. The available Na^+ conductance can be manipulated by various means. One way is to use the Na^+ channel blocker TTX (tetrodoxin). A fraction of Na^+ channels can be blocked by TTX, depending on its concentration, without affecting channel properties (in particular $V_{1/2}$) (Hu et al., 2009). The relation between the available fraction of channels and TTX concentration [TTX] is shown on Fig. 4.16 for hippocampal neurons. This curve, called a *dose-response curve*, can be

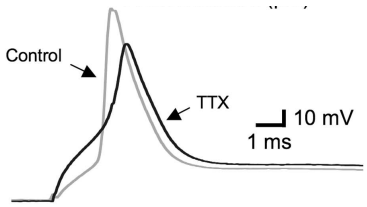

Figure 4.17: Effect on somatic action potential of focal application of TTX on the axonal initiation site (from Palmer and Stuart (2006)).

fitted by a Hill function:

$$f = \frac{1}{1 + \left(\frac{I_{50}}{[\mathrm{TTX}]}\right)^n}$$

where f is the fraction of available (non-blocked) channels, I_{50} is the concentration at which 50% of the channels are blocked, and n is called the Hill coefficient. The data shown in Fig. 4.16 are fitted by a Hill function with $I_{50} = 6.4$ nmol/L and $n = 0.91$; we will assume $n = 1$ for simplicity. The action of TTX may actually depend on the channel subtype. The same measurements were done in Xenopus laevis oocytes where specific channel subtypes were expressed, and the fits gave $I_{50} = 7.8$ nmol/L and $n = 1.2$ for Nav1.6 (the low-voltage subtype expressed in the axonal initial segment), and $I_{50} = 3.8$ nmol/L and $n = 1.2$ for Nav1.2 (another subtype expressed in the AIS) (Rosker et al., 2007).

Several experimental studies report a depolarizing shift in threshold when TTX is applied focally at the AIS. However, TTX concentration was very high, as the goal was to fully block the channels: 500 nM in Kress et al. (2008) and Kress et al. (2010), 10 μM in Colbert and Johnston (1996) and Palmer and Stuart (2006). Combining the data shown in Fig. 4.16 with the threshold equation (using $k = 5$ mV), the expected shifts for 500 nM and 10 μM applications would be 20 and 33 mV, respectively. All these studies report depolarizing shifts in spike threshold, but the quantitative comparison is compromised by at least two issues: 1) TTX application is focal, and the spatial extent of blocking is not tightly controlled (this should reduce the impact of TTX application); 2) spike onset is used as a proxy for spike threshold, but spike shape is greatly degraded with high concentrations of TTX (see Fig. 4.17).

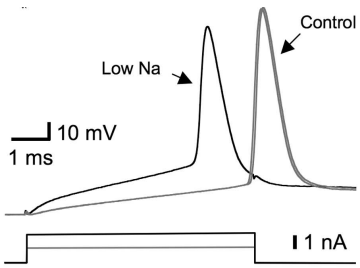

Figure 4.18: Effect on somatic action potential of low sodium application to the axonal initiation site (from Palmer and Stuart (2006)).

Low Na^+ solutions

Another experimental manipulation relevant to the threshold equation is the application of a low Na^+ external solution. The threshold equation predicts that spike threshold should increase because the reversal potential E_{Na} is lower. Specifically, the change in reversal potential should be:

$$\Delta E_{Na} = \frac{RT}{F} \log \frac{[\mathrm{Na}^+]_{\mathrm{new}}}{[\mathrm{Na}^+]_{\mathrm{old}}}$$

In Fig. 4.18, a low Na^+ solution was applied on the axonal initiation site (here 20 μm from the soma), with concentration 25 mM instead of 150 mM in the initial extracellular solution (Palmer and Stuart, 2006). The predicted change in driving force is $\Delta E_{Na} \approx -45$ mV. With $E_{Na} = 70$ mV (calculated using $[\mathrm{Na}^+]_\mathrm{i} = 7$ mM) and $V_{1/2} = -40$ mV, we obtain a predicted change in spike threshold of about 2 mV. The reported change is 4.5 mV on average (the figure shows an example with larger change). Given that the manipulation is local, we can expect that this is an underestimation of the true effect with global change of Na^+ concentration. Thus the change is spike threshold is larger than expected. There is a simple explanation to the discrepancy: changing the extracellular Na^+ concentration also changes the Na^+ conductance g_{Na}. Biophysically, it is clear that g_{Na} should increase when Na^+ concentration increases (more ions, therefore more current). To capture this effect, we need to examine a model that deals with permeability instead of conductance, which we will do in section 4.4.3. Nonetheless, we observe that lowering extracellular Na^+ concentration does have the expected effect of increasing the spike threshold.

Other ways to modulate Na^+ currents

Finally, Na^+ currents can be modulated by phosphorylation by kinases (Astman et al., 1998; Scheuer, 2011; Chen et al., 2008; Wittmack et al., 2005), and by

the action of neuromodulators, for example serotonin, with associated changes in spike threshold (Cotel et al., 2013). However, the currently available data do not allow precise quantification.

4.4.3 The threshold equation with the GHK model

The threshold equation we have derived in section 4.2 was based on a linear model of the Na^+ current (as in the Hodgkin-Huxley model). As this is a phenomenological model, the relation between conductance and ionic concentrations is undetermined. In addition, in some cases it has been shown that the GHK model is a better model of Na^+ currents. This is so in the node of Ranvier of frog myelinated fibers (Dodge and Frankenhaeuser, 1959; Frankenhaeuser, 1960), and one study also reports it in cortical neurons (Baranauskas and Martina, 2006). Here we re-analyze the spike threshold using the GHK model of currents.

We are interested in the value of the Na^+ current near spike initiation, that is, at hyperpolarized voltages. As we have previously seen, the GHK formula for the current is then approximately:

$$I_{Na} \approx P_{Na} \frac{F^2 [Na^+]_o}{RT} V$$

The intuition is that at hyperpolarized potentials, most ions flow inward (the electrical field is directed inward) and so the current should be proportional to the extracellular concentration of Na^+. It should also be proportional to the electrical field across the membrane, and therefore to the membrane potential V. Thus we can write:

$$I_{Na} \approx \lambda_{Na} [Na^+]_o V$$

where λ_{Na} is a constant that depends only on temperature. Note that $\lambda_{Na}[Na^+]_o$ has the dimension of a conductance, and therefore we may define $g_{Na} = \lambda_{Na}[Na^+]_o$. Using the exponential model, the membrane equation is then:

$$C\frac{dV}{dt} = g_L(E_L - V) + \lambda_{Na} e^{(V-V_{1/2})/k} [Na^+]_o V + I$$

We can then make the same approximation as previously and replace the factor V that modulates the exponential by $V_{1/2}$ (although this is less accurate). We then obtain the same membrane equation as before for the threshold, with

$$\theta = V_{1/2} - k \log \left(\frac{\lambda_{Na}}{g_L} [Na^+]_o \frac{V_{1/2}}{k} \right)$$

This updated equation makes the dependence on $[Na^+]_o$ appear explicitly. We can now make a meaningful prediction for the experiment with low Na^+ application (Palmer and Stuart, 2006). In that study, a solution with 25 mM instead of 150 mM Na^+ was applied locally to the axonal initiation site. The theoretical prediction is a shift in spike threshold of

$$\Delta\theta = k \log \frac{[\mathrm{Na}^+]_{\mathrm{new}}}{[\mathrm{Na}^+]_{\mathrm{old}}}$$

and here, with $k = 5$ mV, we find about 9 mV. The reported change was 4.5 mV on average. However the application was local, and we may expect that the threshold shift is smaller than with a global application.

4.5 What are the conditions for excitability?

4.5.1 How many channels make a cell excitable?

In the sharp model

It is clear that if there are too few Na^+ channels, then the cell cannot be excitable. The minimum required number of channels can be easily calculated in the sharp model (Fig. 4.10A). Just above $V_{1/2}$, the membrane current is:

$$I(V_{1/2}^+) = g_L(E_L - V_{1/2}) + g_{Na}(E_{Na} - V_{1/2})$$

This must be positive for the cell to be excitable. Therefore, the ratio of Na^+ to leak conductance, which we denote p, must be such that[20]:

$$p \equiv \frac{g_{Na}}{g_L} > \frac{V_{1/2} - E_L}{E_{Na} - V_{1/2}}$$

To give an order of magnitude, we can choose $E_{Na} = 70$ mV, $V_{1/2} = -30$ mV and $E_L = -70$ mV. We then obtain $p > 0.4$.

In this model, the Na^+ conductance can be increased indefinitely without destabilizing the resting potential. This is so because there is no Na^+ current below $V_{1/2}$. However, in reality, there is a small but positive Na^+ current below $V_{1/2}$, and increasing the Na^+ conductance should at some point make the resting potential disappear — the cell spikes and never rests. This effect is captured in the Boltzmann model[21].

In the Boltzmann model

With the Boltzmann model, excitability for slow and fast inputs are not equivalent. Here we choose the definition for fast inputs, but similar calculations can be carried out with slow inputs. Thus the model is said to be excitable if it has two stable equilibria; the unstable equilibrium is the spike threshold.

When $g_{Na} = 0$, there is a single stable equilibrium, the resting potential. If g_{Na} is increased sufficiently, another equilibrium appears. This event is what we have previously called a *bifurcation* (section 4.1.4). We illustrate it on Fig. 4.19, where we show the membrane current $I(V)$ divided by g_L, as a function of V, for different values of the conductance ratio $p = g_{Na}/g_L$.

We can see that the switch from one equilibrium to two and three occurs when the excitability curve is tangent to the horizontal axis, that is, $I(V) = I'(V) = 0$. This pair of equations can be solved exactly for p (see Appendix **??**):

$$p = \frac{(V - E_L)^2}{(E_{Na} - V)(V - E_L) - k(E_{Na} - E_L)}$$

where V is a solution to this pair of equations (voltage where the excitability curve is tangent to the horizontal axis). If we replace V by $V_{1/2}$, we obtain the following approximation:

$$p = \frac{V_{1/2} - E_L}{E_{Na} - V_{1/2} - k\frac{E_{Na} - E_L}{V_{1/2} - E_L}}$$

[20] Another expression can be derived with the GHK model.

[21] Note that the exponential model cannot be used for this question because this model is always excitable as soon as $g_{Na} > 0$, since the Na^+ current is unbounded.

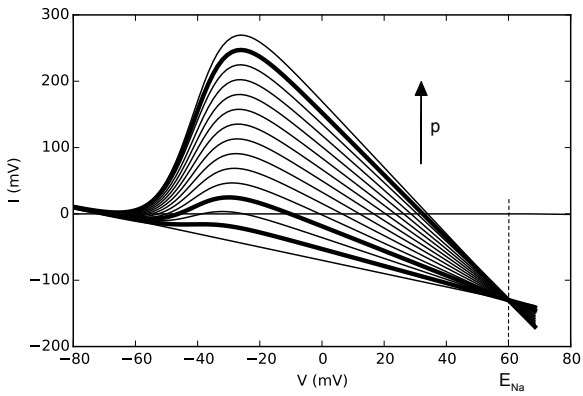

Figure 4.19: Excitability curve $I(V)/g_L$ of the Boltzmann model, where $p = g_{Na}/g_L$ is varied.

With the same values as before and $k = 5$ mV, we obtain $p \approx 0.48$, higher than in the sharp model, but with the same order of magnitude. A more accurate approximation can be derived (see Appendix **??**), giving $p \approx 0.61$.

We can use exactly the same reasoning to derive the maximum number of channels that allow a stable resting potential. On Fig. 4.19, this corresponds to one of the upper curves, where the minimum is tangent to the horizontal axis. This corresponds to exactly the same mathematical conditions, and therefore the same equation of p as a function of V, but V is not the same. In particular, V is not close to $V_{1/2}$ but rather to E_L.

To calculate the solution for p, the trick is to first get an estimate of V. This can be done with the Boltzmann model, but in fact, as we have seen in section 4.3.3, a good approximation in hyperpolarized voltages is the exponential model, which is simpler. In the exponential model, the activation function (an exponential) satisfies $m' = m/k$. Therefore the equations $I(V) = I'(V) = 0$ mean:

$$\begin{aligned} E_L - V + pm(E_{Na} - V) &= 0 \\ -1 + pm/k(E_{Na} - V) - pm &= 0 \end{aligned}$$

We obtain pm from the first equation and replace in the second equation. We then obtain $V \approx E_L + k$. It follows that maximum conductance ratio is

$$p = \frac{k}{m(E_{Na} - E_L)} = \frac{k}{(E_{Na} - E_L)} e^{\frac{V_{1/2} - E_L}{k} - 1}$$

With the same values as before, we obtain $p \approx 39$. Thus, in the Boltzmann model, the cell is excitable and has a resting potential when $0.6 < p < 39$. Incidentally, we have also found that the spike threshold is always greater than $E_L + k$, and the resting potential cannot be higher than $E_L + k$. The condition for the minimum conductance ratio also gives the maximum spike threshold that can be obtained (see Appendix **??**).

4.5.2 What channel properties are compatible with excitability?

The range of conductance ratios compatible with excitability depends on channel properties. Under what conditions is this range not empty? For example, if the activation curve were very smooth (large k), then we might not be able to find any value of the Na^+ conductance that leads to several equilibria. We can approach this question again with bifurcation theory. We have seen that the minimum and maximum conductance ratios are such that $I(V) = I'(V) = 0$. This pair of solutions disappears at a bifurcation point, where we must then have $I''(V) = 0$. In the Boltzmann model, this set of 3 equations leads to $V_{1/2} \approx E_L + 2k$. This has been derived in (Angelino and Brenner, 2007) (see Appendix **??**). Thus, for the cell to be excitable and have a resting potential, channel properties must satisfy: $V_{1/2} > E_L + 2k$.

In other words, the activation curve of Na^+ channels must be sharp enough. With $E_L = -70$ mV and $V_{1/2} = -30$ mV, we obtain the condition $k < 20$ mV, which is met by Na^+ channels measured in patch clamp (Fig. 4.11).

Bibliography

Angelino, E. and Brenner, M. P. (2007). Excitability constraints on voltage-gated sodium channels. *PLoS computational biology*, 3(9):1751–60.

Astman, N., Gutnick, M. J., and Fleidervish, I. A. (1998). Activation of Protein Kinase C Increases Neuronal Excitability by Regulating Persistent Na+ Current in Mouse Neocortical Slices. *Journal of Neurophysiology*, 80(3):1547–1551.

Azouz, R. and Gray, C. M. (1999). Cellular mechanisms contributing to response variability of cortical neurons in vivo. *J Neurosci*, 19(6):2209–23. undefined Mar 15 Cellular mechanisms contributing to response variability of cortical neurons in vivo 10066274 0270-6474 Journal Article http://www.ncbi.nlm.nih.gov/entrez/query.fcgi?cmd=Retrieve&db=PubMed&dopt=Citation&list_uids=10066274 The Center for Neuroscience, Physiology, and Behavior, University of California, Davis, California 95616, USA.

Badel, L., Lefort, S., Brette, R., Petersen, C. C. H., Gerstner, W., and Richardson, M. J. E. (2008). Dynamic I-V curves are reliable predictors of naturalistic pyramidal-neuron voltage traces. *Journal of Neurophysiology*, 99(2):656–66.

Baranauskas, G. and Martina, M. (2006). Sodium Currents Activate without a Hodgkin and Huxley-Type Delay in Central Mammalian Neurons. *Journal of Neuroscience*, 26(2):671–684.

Brette, R. and Gerstner, W. (2005). Adaptive exponential integrate-and-fire model as an effective description of neuronal activity. *Journal of Neurophysiology*, 94(5):3637–42.

Carter, B. C. and Bean, B. P. (2009). Sodium entry during action potentials of mammalian central neurons: incomplete inactivation and reduced metabolic efficiency in fast-spiking neurons. *Neuron*, 64(6):898–909.

Chen, Y., Yu, F. H., Sharp, E. M., Beacham, D., Scheuer, T., and Catterall, W. A. (2008). Functional properties and differential neuromodulation of Nav1.6 channels. *Molecular and Cellular Neuroscience*, 38(4):607–615.

Colbert, C. M. and Johnston, D. (1996). Axonal Action-Potential Initiation and Na+ Channel Densities in the Soma and Axon Initial Segment of Subicular Pyramidal Neurons. *The Journal of Neuroscience*, 16(21):6676–6686.

Cotel, F., Exley, R., Cragg, S. J., and Perrier, J.-F. (2013). Serotonin spillover onto the axon initial segment of motoneurons induces central fatigue by inhibiting action potential initiation. *Proceedings of the National Academy of Sciences of the United States of America*, 110(12):4774–4779.

Dodge, F. A. and Frankenhaeuser, B. (1959). Sodium currents in the myelinated nerve fibre of Xenopus laevis investigated with the voltage clamp technique. *The Journal of Physiology*, 148(1):188–200.

Fourcaud-Trocme, N., Hansel, D., van Vreeswijk, C., and Brunel, N. (2003). How spike generation mechanisms determine the neuronal response to fluctuating inputs. *J neurosci*, 23(37):11628–40. undefined Dec 17 How spike generation mechanisms determine the neuronal response to fluctuating inputs 14684865 1529-2401 Journal Article http://www.ncbi.nlm.nih.gov/entrez/query.fcgi?cmd=Retrieve&db=PubMed&dopt=Citation&list_uids=146 Centre National de la Recherche Scientifique Unite Mixte de Recherche 8119, Neurophysique et Physiologie du Systeme Moteur, Unite de Formation et de Recherche Biomedicale, Universite Paris 5 Rene Descartes, 75270 Paris Cedex 06, France.

Frankenhaeuser, B. (1960). Sodium permeability in toad nerve and in squid nerve. *The Journal of Physiology*, 152(1):159–166.

Hallermann, S., de Kock, C. P. J., Stuart, G. J., and Kole, M. H. P. (2012). State and location dependence of action potential metabolic cost in cortical pyramidal neurons. *Nature Neuroscience*, 15(7):1007–1014.

Harrison, P. M., Badel, L., Wall, M. J., and Richardson, M. J. E. (2015). Experimentally Verified Parameter Sets for Modelling Heterogeneous Neocortical Pyramidal-Cell Populations. *PLOS Computational Biology*, 11(8):e1004165.

Henze, D. A. and Buzsaki, G. (2001). Action potential threshold of hippocampal pyramidal cells in vivo is increased by recent spiking activity. *Neuroscience*, 105(1):121–30. undefined Action potential threshold of hippocampal pyramidal cells in vivo is increased by recent spiking activity 11483306 0306-4522 Journal Article http://www.ncbi.nlm.nih.gov/entrez/query.fcgi?cmd=Retrieve&db=PubMed&dopt=Citation&list_uids=114 Center for Molecular and Behavioral Neuroscience, Rutgers, The State University of New Jersey, 197 University Avenue, Newark, NJ 07102, USA.

Hodgkin, A. and Huxley, A. (1952a). A quantitative description of membrane current and its application to conduction and excitation in nerve. *J Physiol (Lond)*, 117:500.

Hodgkin, A. L. and Huxley, A. F. (1952b). Currents carried by sodium and potassium ions through the membrane of the giant axon of Loligo. *The Journal of Physiology*, 116(4):449–472.

Hu, W., Tian, C., Li, T., Yang, M., Hou, H., and Shu, Y. (2009). Distinct contributions of Na(v)1.6 and Na(v)1.2 in action potential initiation and backpropagation. *Nat Neurosci*, 12(8):996–1002.

Koch, C., Bernander, O., and Douglas, R. J. (1995). Do neurons have a voltage or a current threshold for action potential initiation? *Journal of Computational Neuroscience*, 2(1):63–82.

Kole, M. H. P. and Stuart, G. J. (2008). Is action potential threshold lowest in the axon? *Nat Neurosci*, 11(11):1253–1255.

Kress, G. J., Dowling, M. J., Eisenman, L. N., and Mennerick, S. (2010). Axonal sodium channel distribution shapes the depolarized action potential threshold of dentate granule neurons. *Hippocampus*, 20(4):558–571.

Kress, G. J., Dowling, M. J., Meeks, J. P., and Mennerick, S. (2008). High Threshold, Proximal Initiation, and Slow Conduction Velocity of Action Potentials in Dentate Granule Neuron Mossy Fibers. *Journal of Neurophysiology*, 100(1):281–291.

Lapicque, L. (1907). Recherches quantitatives sur l'excitation lectrique des nerfs traite comme une polarisation. *J physiol pathol gen*, 9:620–635. undefined Recherches quantitatives sur l'excitation lectrique des nerfs traite comme une polarisation J physiol pathol gen.

Levitan, I. B. (1994). Modulation of ION Channels by Protein Phosphorylation and Dephosphorylation. *Annual Review of Physiology*, 56(1):193–212.

Madeja, M. (2000). Do neurons have a reserve of sodium channels for the generation of action potentials? A study on acutely isolated CA1 neurons from the guinea-pig hippocampus. *European Journal of Neuroscience*, 12(1):1–7.

Morris, C. and Lecar, H. (1981). Voltage oscillations in the barnacle giant muscle fiber. *Biophysical Journal*, 35(1):193–213.

Nagumo, J. S., Arimoto, S., and Yoshizawa, S. (1962). An active pulse transmission line simulating nerve axon. volume 50, pages 2061–2071. undefined Proc. IRE An active pulse transmission line simulating nerve axon.

Palmer, L. M. and Stuart, G. J. (2006). Site of Action Potential Initiation in Layer 5 Pyramidal Neurons. *The Journal of Neuroscience*, 26(6):1854–1863.

Platkiewicz, J. and Brette, R. (2010). A threshold equation for action potential initiation. *PLoS Computational Biology*, 6(7):e1000850.

Rosker, C., Lohberger, B., Hofer, D., Steinecker, B., Quasthoff, S., and Schreibmayer, W. (2007). The TTX metabolite 4,9-anhydro-TTX is a highly specific blocker of the Nav1.6 voltage-dependent sodium channel. *American Journal of Physiology - Cell Physiology*, 293(2):C783–C789.

Rossant, C., Goodman, D. F. M., Fontaine, B., Platkiewicz, J., Magnusson, A. K., and Brette, R. (2011). Fitting neuron models to spike trains. *Frontiers in Neuroscience*, 5:9.

Rossant, C., Goodman, D. F. M., Platkiewicz, J., and Brette, R. (2010). Automatic fitting of spiking neuron models to electrophysiological recordings. *Frontiers in Neuroinformatics*, 4:2.

Scheuer, T. (2011). Regulation of sodium channel activity by phosphorylation. *Seminars in Cell & Developmental Biology*, 22(2):160–165.

Schmidt-Hieber, C. and Bischofberger, J. (2010). Fast Sodium Channel Gating Supports Localized and Efficient Axonal Action Potential Initiation. *Journal of Neuroscience*, 30(30):10233–10242.

Sekerli, M., Del Negro, C. A., Lee, R. H., and Butera, R. J. (2004). Estimating action potential thresholds from neuronal time-series: new metrics and evaluation of methodologies. *IEEE transactions on bio-medical engineering*, 51(9):1665–1672.

Sloper, J. J. and Powell, T. P. S. (1979). A Study of the Axon Initial Segment and Proximal Axon of Neurons in the Primate Motor and Somatic Sensory Cortices. *Philosophical Transactions of the Royal Society of London. Series B, Biological Sciences*, 285(1006):173–197.

Wilent, W. B. and Contreras, D. (2005). Stimulus-dependent changes in spike threshold enhance feature selectivity in rat barrel cortex neurons. *J Neurosci*, 25(11):2983–91. undefined Mar 16 Stimulus-dependent changes in spike threshold enhance feature selectivity in rat barrel cortex neurons 15772358 1529-2401 Journal Article

http://www.ncbi.nlm.nih.gov/entrez/query.fcgi?cmd=Retrieve&db=PubMed&dopt=Citation&list_uids=157
Department of Neuroscience, University of Pennsylvania School of Medicine, Philadelphia, Pennsylvania 19106-6074, USA.

Wittmack, E. K., Rush, A. M., Hudmon, A., Waxman, S. G., and Dib-Hajj, S. D. (2005). Voltage-Gated Sodium Channel Nav1.6 Is Modulated by p38 Mitogen-Activated Protein Kinase. *Journal of Neuroscience*, 25(28):6621–6630.

List of Figures

Index